JOURNAL OF GEOPHYSICAL RESEARCH, VOL. 113, A02202, doi:10.1029/2007JA012600, 2008

Spectral morphology of the X-ray emission from Jupiter's aurorae

G. Branduardi-Raymont,[1] R. F. Elsner,[2] M. Galand,[3] D. Grodent,[4] T. E. Cravens,[5] P. Ford,[6] G. R. Gladstone,[7] and J. H. Waite Jr.[7]

Received 18 June 2007; revised 24 August 2007; accepted 24 October 2007; published 2 February 2008.

[1] Simultaneous Chandra X-ray and Hubble Space Telescope FUV observations of Jupiter's aurorae carried out in February 2003 have been re-examined to investigate the spatial morphology of the X-ray events in different energy bands. The data clearly show that in the Northern auroral region (in the main auroral oval and the polar cap) events with energy > 2 keV are located at the periphery of those with energy < 2 keV and coincide with FUV bright features. In addition, X-ray spectra extracted from the areas where the two event distributions are concentrated possess different shapes. We associate the > 2 keV events (~45 MW emitted power) with the electron bremsstrahlung component recently revealed by XMM-Newton in the spectra of Jupiter's aurorae, and the < 2 keV emission (~230 MW) with the product of ion charge exchange, now established as the likely mechanism responsible for the soft X-ray Jovian aurora. We suggest that the same population of energetic electrons may be responsible for both, the X-ray bremsstrahlung and the FUV emission of Jupiter's aurorae. Comparison of the > 2 keV X-ray and FUV (340 GW) powers measured during the observations shows that they are broadly consistent with the predicted emissions from a population of energetic electrons precipitating in the planet's atmosphere, thus supporting our interpretation.

Citation: Branduardi-Raymont, G., R. F. Elsner, M. Galand, D. Grodent, T. E. Cravens, P. Ford, G. R. Gladstone, and J. H. Waite Jr. (2008), Spectral morphology of the X-ray emission from Jupiter's aurorae, *J. Geophys. Res.*, *113*, A02202, doi:10.1029/2007JA012600.

1. Introduction and Motivation

[2] Spectroscopic studies of the X-ray emission from planetary atmospheres provide a novel way to explore the characteristics of the radiating energetic particles, of their acceleration mechanisms and their response to solar activity [a comprehensive review is presented by *Bhardwaj et al.*, 2007]. Recent observations with XMM-Newton have revealed the presence of a high energy component in the X-ray spectra of Jupiter's aurorae [*Branduardi-Raymont et al.*, 2007]. Unlike below 2 keV, where the spectrum indicates the presence of emission lines consistent with heavy ion precipitation [see also *Branduardi-Raymont et al.*, 2004; *Elsner et al.*, 2005], at higher energies a continuum is observed, characteristic of bremsstrahlung emission produced by electron precipitation. This spectral component, also observed to be strongly variable, had been predicted and modeled theoretically [e.g., *Waite et al.*, 1992; *Singhal et al.*, 1992]. The very flat X-ray power law observed on one occasion with XMM-Newton suggests that the precipitating electron energy distribution may not always be Maxwellian (as assumed in some models, e.g., *Grodent et al.*, 2001), but at times, probably following powerful acceleration in Jupiter's magnetosphere, may take a different shape. The emission below 2 keV was also observed to vary on the same occasion, although there is no clear indication of a correlation in the behavior of the electron and ion populations. What is clear is that the time when XMM-Newton observed the variability coincided with a period of intense solar activity in November 2003. This raises the question of how the two particle populations and their energetics are affected by solar wind conditions, how different may be their response to changes in Jupiter's magnetospheric environment, and of how they may interact on their separate ways to producing X-ray emission. It is interesting to consider, for example, whether and how their footprints may be separated in the auroral regions, i.e., how the low and high energy X-rays may be spatially distributed over Jupiter's auroral oval and polar cap.

[3] Turning to the ultraviolet band, the existence of a FUV aurora on Jupiter was first recognized by the Voyager Ultraviolet Spectrometer (UVS) and attributed to H_2 Lyman and Werner bands and to H Lyα emissions [*Broadfoot et al.*, 1979; *Sandel et al.*, 1979]. The brightnesses observed are

[1] Mullard Space Science Laboratory, University College London, Holmbury St. Mary, UK.
[2] NASA Marshall Space Flight Center, NSSTC/XD12, Space Science Branch, Huntsville, Alabama, USA.
[3] Imperial College London, Space and Atmospheric Physics Group, Blackett Laboratory, London, UK.
[4] Laboratoire de Physique Atmosphérique et Planétaire, Institut d'Astrophysique et de Géophysique, Université de Liège, Liège, Belgium.
[5] Department of Physics and Astronomy, University of Kansas, Lawrence, Kansas, USA.
[6] Massachusetts Institute of Technology, Kavli Institute for Astrophysics and Space Research, Cambridge, Massachusetts, USA.
[7] Southwest Research Institute, San Antonio, Texas, USA.

0148-0227/08/2007JA012600$09.00

consistent with excitation of the atmospheric species (H_2, H) by electrons of energies of the order of few 10s to 100 keV [*Singhal et al.*, 1992]. Alternative excitation mechanisms involving protons and heavy ions have been proposed, but have difficulties in explaining the data (*Elsner et al.*, 2005; see also *Bhardwaj and Gladstone*, 2000 for a comprehensive review of observations and models of the Jovian aurora). The FUV intensities and spectral characteristics were used, in conjunction with modeling techniques, to predict the X-ray bremsstrahlung fluxes expected from the energetic electrons producing the FUV aurora, and expected to be detected at Jupiter by the Ulysses spacecraft instrumentation [*Waite et al.*, 1992]. While Ulysses returned only hard X-ray upper limits [*Hurley et al.*, 1993], the electron energies implied by the FUV aurora [30 to 200 keV, *Gustin et al.*, 2004] are consistent with those (several tens of keV) inferred for the electrons thought to generate the high energy X-ray bremsstrahlung observed by XMM-Newton [*Branduardi-Raymont et al.*, 2007]. The obvious question is then whether the same electron population may be responsible for both, FUV emission and X-ray bremsstrahlung from the aurorae. One way to try and answer this is again by comparing the spatial distribution of the hard X-ray and FUV photons, ideally at the same time.

[4] Making progress on the issues highlighted above requires high spatial resolution, given that the whole disk of Jupiter has a diameter of only ~40 arcsec on average. In the X-rays XMM-Newton offers high sensitivity but insufficient spatial resolution (Point Spread Function, PSF, of ~15 arcsec Half Energy Width, or HEW), while the Chandra X-ray Observatory (CXO) provides much sharper images (~0.8 arcsec HEW) but lower photon fluxes (effective area at 1 keV some 5 times lower than XMM-Newton); this is an important factor, especially if the emission is to be separated into different energy bands. With this in mind we have re-examined the CXO observations of Jupiter carried out in February 2003 [*Elsner et al.*, 2005] in order to study the spatial distribution of the X-ray emission. The observations were executed simultaneously with FUV measurements by the Hubble Space Telescope (HST) Imaging Spectrograph (STIS): during these a strong FUV flare was detected within the Northern polar cap, and was found to be associated with an enhancement in the 0.25–2.0 keV X-ray emission.

[5] In the present paper we report the results of this study of Jupiter's auroral regions. In section 2 we describe the spatial distributions of the CXO X-ray events at energies below and above 2 keV, and we show how the X-ray emission is mapped with respect to the FUV morphology; we also present model fits to the CXO spectra extracted from the inner and outer parts of the Northern auroral region. In section 3 we discuss our results and compare the relative energetics in the X-ray and FUV bands with model predictions. Finally we summarize our conclusions in section 4.

2. Observations

[6] The CXO observed Jupiter on 24–26 February 2003 for four rotations of the planet (~40 h). Details of the observations and analysis techniques are reported by *Elsner et al.* [2005]. Here we focus only on data from ACIS-S (Advanced CCD Imaging Spectrometer) which provides high spatial resolution (PSF of 0.5 arcsec Full Width Half Maximum) as well as good, CCD-quality spectral discrimination.

[7] Figure 1 presents the distribution of X-ray events in three energy bands for the System III Northern and Southern hemispheres of Jupiter, for the whole of the ACIS-S observations. The associated exposure maps are also shown in Figure 1, as well as close-up views of the Northern and Southern auroral regions. The numbers of counts detected respectively in the Northern and Southern hemispheres are 839 and 596 (0.3–1.0 keV), 208 and 190 (1.0–2.0 keV) and 83 and 59 (2.0–8.0 keV). Although the number of events above 2 keV is relatively small, it is clear that in the Northern hemisphere the high energy (> 2 keV) events (in blue) show a very different spatial distribution from the auroral events below 1 keV (grey), and lie at the periphery of the distribution of lower energy events. The blue ellipses in the Northern hemisphere close-up panel are placed by eye and drawn as to maximize the content of events of the two types, soft X-rays inside the inner ellipse and harder ones in between the two. Events below the blue horizontal line in the same panel were disregarded in the spectral extraction (see below) as there are too few of them. This dearth of events is simply a viewing projection effect due to the small grazing angle with which the CXO must view Jupiter's Northern polar regions. Figure 2 illustrates how the area below the blue horizontal line in the Northern hemisphere close-up polar projection of Figure 1 maps to a very narrow strip close to the planet's limb in sky coordinates.

[8] About half of the > 2 keV events in the top left panel of Figure 1 are distributed within the red contour strip defined by the L = 5.9 (Io) and L = 30 footprints (according to the VIP4 model magnetosphere, *Connerney et al.*, 1998), are centered on Central Meridian Longitude (CML) = 210° and are thus coincident with a section of the FUV main auroral oval as shown in Figure 2 of *Gladstone et al.* [2002]. The rest are concentrated around CML = 160°, just inside

Figure 1. Top left: Distribution of ACIS-S events in Jupiter's System III Northern hemisphere. Events with nominal energies in the band 0.3–1.0 keV are shown in grey, those in the band 1.0–2.0 keV in green, and those in the band 2.0–8.0 keV in blue. The dotted straight lines show constant System III longitude in 30° steps, while the dotted circles show the 30° and 60° latitudes. Grey contours, with numerical labels, mark constant surface VIP4 model magnetic field strength in Gauss, and the red contours mark the Io L = 5.9 and the L = 30 flux tubes. Top right: Close-up of the Northern auroral region (outlined by the rectangle in the panel on the left). Blue ellipses have been added, placed by eye to define regions that maximize the content of events of the two types, soft X-rays inside the inner ellipse, and harder ones in between the two. The region below the horizontal blue line is excluded from the spectral results given in Table 1 and displayed in Figure 7. Middle left: Same as top left, but for the Southern hemisphere. Middle right: Close-up of the Southern auroral region. Bottom: ACIS-S exposure maps for Jupiter's System III Northern (left) and Southern (right) hemispheres.

the L = 30 contour, and co-located with some of the brightest areas of FUV emission in the same figure of Gladstone et al. The number of events in the Southern auroral region in Figure 1 is even smaller than in the North, but the distributions appear to be at least consistent with the Northern aurora scenario. This result cannot be an artifact of unequal exposure times (see bottom panel of Figure 1): the minimum and maximum exposure durations were 25.7 and 39.5 ks in the System III Northern hemisphere and 22.0 and 35.8 ks in the South. We can also exclude that the effect be produced by the presence of background events, which we have not subtracted. In this we have followed the approach taken by *Elsner et al.* [2005] in their analysis of the 0.3–2.0 keV emission from Jupiter: they found the background

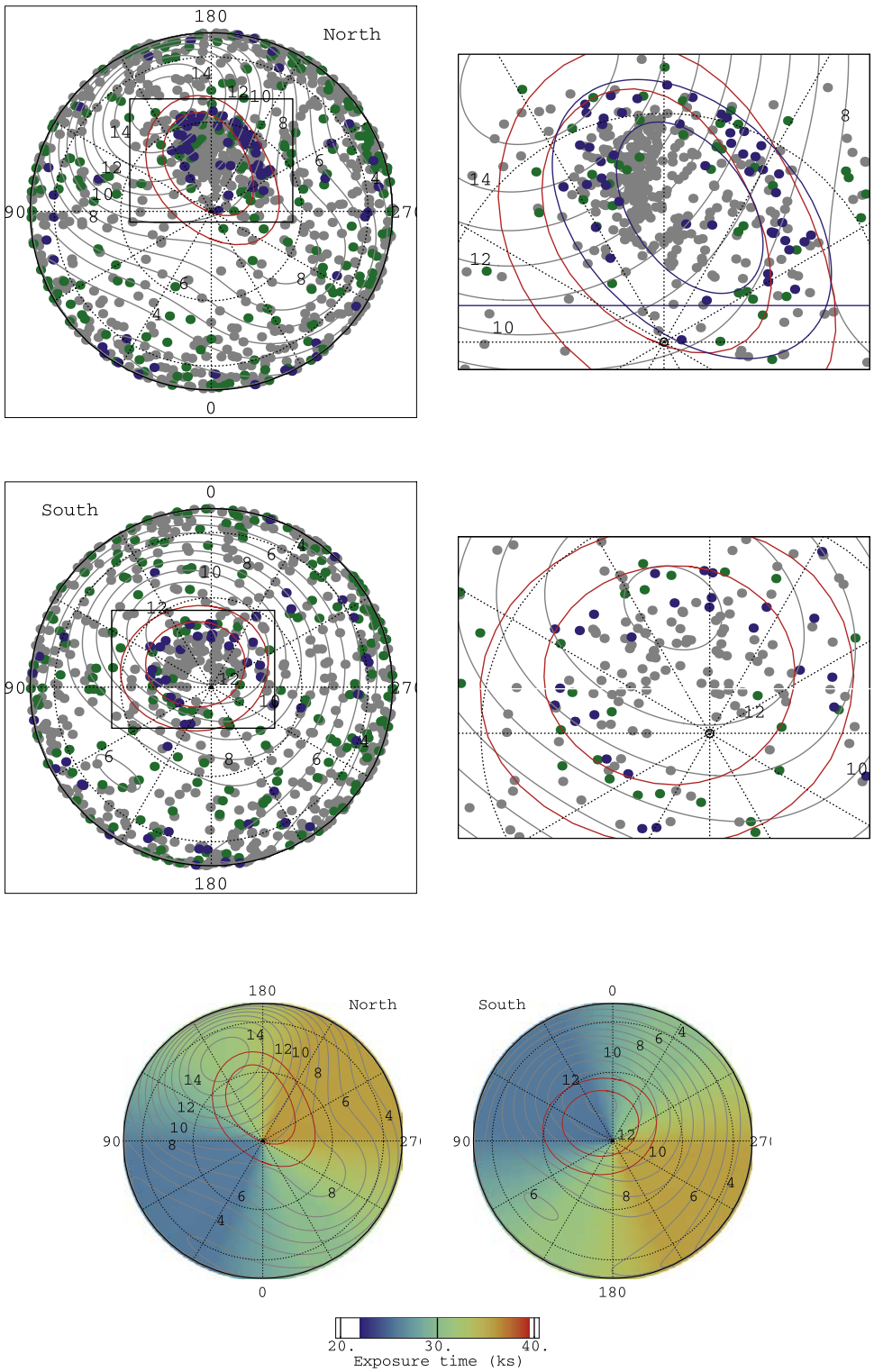

Figure 1

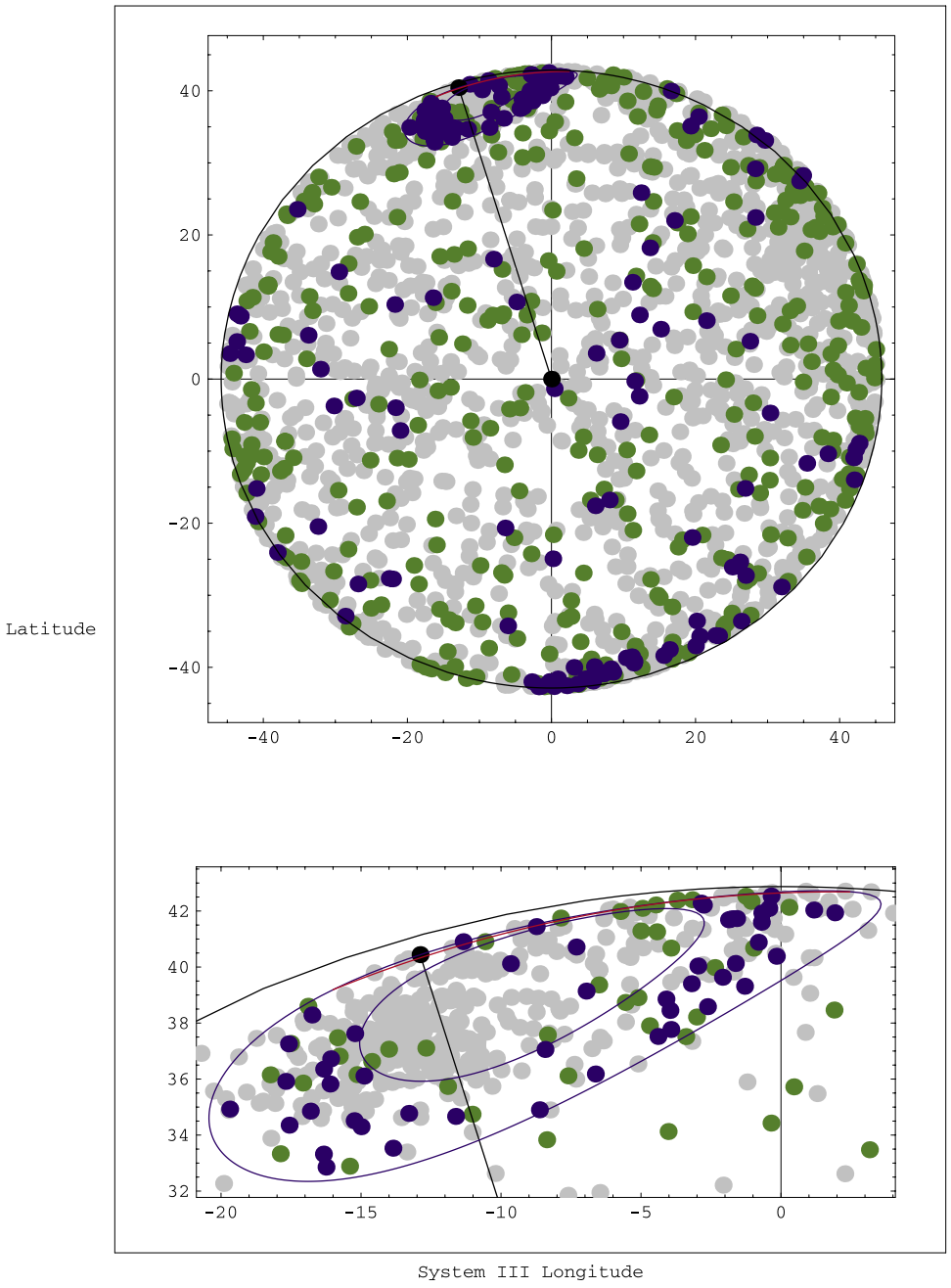

Figure 2. Top: X-ray events from the polar plots in Figure 1 transformed to sky coordinates in Jupiter's frame assuming a CML of 175°. Events with energies in the band 0.3–1.0 keV are shown in grey, those in the band 1.0–2.0 keV in green, and those in the band 2.0–8.0 keV in blue. The blue contours are the transformed boundaries of the inner and outer ellipses (blue in the top right panel of Figure 1), and the red curve is the transformed horizontal blue line from the same panel of Figure 1. The two black dots show the sub-observer point (at the origin) and the position of the North pole. Bottom: Close-up of the Northern auroral region.

level to be less than 3% of the planet's emission in this energy band and thus neglected it. Moreover, the body of the planet blocks X-rays from cosmic sources farther away. For the 2.0–8.0 keV range, we have carefully investigated the importance of the background. From the region enclosed between 2 and 5 Jupiter radii centered on the planet, we estimate a background rate of $(0.19 \pm 0.02) \times 10^{-6}$ cts s^{-1} $pixel^{-1}$; this has to be compared with a rate of $(16.1 \pm 2.4) \times 10^{-6}$ cts s^{-1} $pixel^{-1}$ detected in the area between the two blue ellipses and above the blue horizontal line in the top right panel of Figure 1. We conclude that it is reasonable to neglect background subtraction in the North auroral region.

[9] Figure 3 shows cylindrical projection count rate maps in System III coordinates for the energy bands 0.3–2.0 keV (top) and 2.0–8.0 keV (bottom). The maps were constructed in the following way: For each of the energy bands

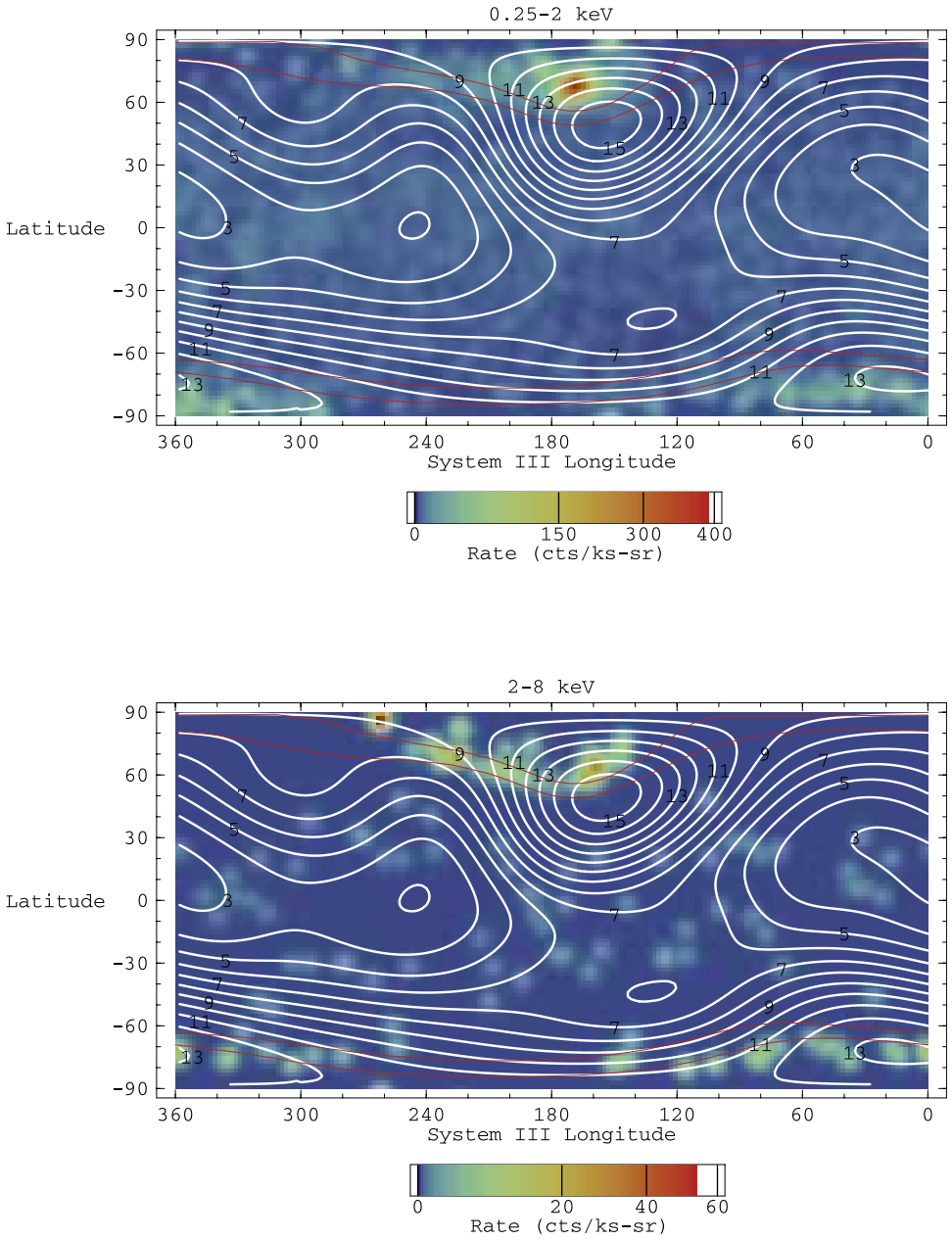

Figure 3. Cylindrical projections of the ACIS-S count rate maps in the energy bands 0.25–2.0 keV (top) and 2.0–8.0 keV (bottom). The labeled white contours mark constant surface VIP4 model magnetic field strength in Gauss. The red lines are the Io and L = 30 flux tube footprints.

0.25–2.0 keV and 2.0–8.0 keV, events were binned by System III longitude and latitude in 2° × 2° bins. Rates were determined by dividing the number of events by the appropriate exposure time and solid angle as viewed from the center of the planet. The latter varies with latitude, but not with longitude, as

$$\Omega_{bin}(\alpha_1, \alpha_2) = \frac{\Delta\phi}{2\pi}(\cos\alpha_1 - \cos\alpha_2)$$

where α_1 and α_2 are the latitudes bounding the bin ($\alpha = \pi/2$ at the North pole), $\alpha_1 - \alpha_2 = \Delta\phi$ and $\Delta\phi$ equals 2° expressed in radians. The resulting cylindrical projection was then convolved with a 2-D Gaussian with $\sigma = 1.5\Delta\phi$ in each dimension. These count rate maps clearly reinforce the conclusion that the events below and above 2 keV display a different spatial distribution.

[10] As mentioned in section 1, the CXO observations of February 2003 were carried out simultaneously with Hubble STIS FUV measurements of the Northern aurora, so we can make a direct comparison of the spatial distribution of the X-ray photons with that of the FUV emission in this region. Figure 4 shows a polar projection of the STIS FUV image taken on 24 February 2003, 19:41 UT (see *Elsner et al.*, 2005 for details), with all the X-ray photons detected during the complete CXO observation overplotted. The small green

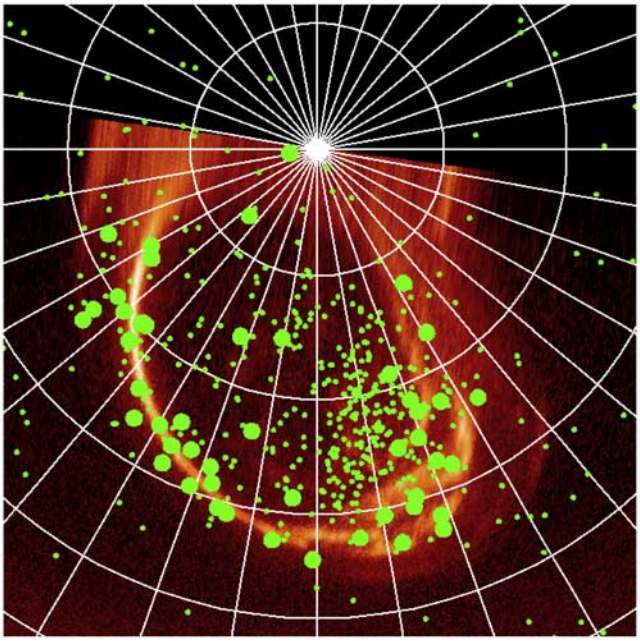

Figure 4. Polar projection of one of the Hubble STIS FUV images of Jupiter's Northern aurora taken on 24 February 2003; overplotted are all the X-ray photons detected by the CXO during its simultaneous observation. Small green dots: < 2 keV photons. Large green dots: > 2 keV photons. The 10° spaced grid is fixed in System III with 180° toward the bottom and 90° to the right.

dots represent X-ray photons with energy < 2 keV, the big green dots those with energy > 2 keV. Most of the > 2 keV photons are very well aligned with the FUV main oval, suggesting that in this region the same high energy electrons produce X-ray and FUV emissions at the same time. The < 2 keV photons appear co-located in the 'active region' [*Grodent et al.*, 2004] which lies poleward of the main oval; very surprisingly, the CXO data do not show the presence of high energy X-ray photons in this area. However, the FUV-dark region also appears dark in the X-rays. Figure 5 (with the same plotting conventions as Figure 4) displays the X-ray photons collected by the CXO during individual orbits of HST, overplotted on the first of several STIS exposures obtained over the same HST orbit (~40 min). The X-ray statistics are clearly poorer than in Figure 4, but the different morphologies of the low and high energy X-ray photons, and the coincidence of the > 2 keV events with FUV bright features, are even more striking.

[11] Figure 6 displays the distribution of count rates versus latitude on Jupiter in the energy bands 0.3–1.0 keV, 1.0–2.0 keV and 2.0–8.0 keV. These distributions are normalized so that a uniform disk would yield a flat distribution. The high-latitude peaks are a signature of the aurorae. The auroral signal is very strong in the 0.3–1.0 keV range; it appears mostly absent in the 1.0–2.0 keV panel, but is again clearly present in the 2.0–8.0 keV band. The reduction in the 1.0–2.0 keV auroral events indicates a real dichotomy in the energy distribution of the X-ray photons, consistent with the idea that events at energies < 1 keV originate from ionic charge exchange, and those at > 2 keV from electron bremsstrahlung. However, in interpreting these results one should keep in mind the presence of the disk contribution from scattered solar X-rays, in addition to any auroral ion and electron precipitation effects [*Branduardi-Raymont et al.*, 2004; *Bhardwaj et al.*, 2006].

[12] Figure 7 shows two count rate spectra: one (in grey) is extracted from the region inside the inner blue ellipse in the top right panel of Figure 1, the other (blue) is from the area between the two blue ellipses. As stated earlier, the blue ellipses were drawn so as to approximately maximize the number of soft X-rays inside the inner ellipse and that of harder ones in between the two; also, the very few events below the blue horizontal line in the same panel of Figure 1 were disregarded. The spectra are as observed, i.e., have not been corrected for the effective area and energy resolution of the High Resolution Mirror Assembly (HRMA)/ACIS-S combination. It is clear that the two spectra are different, with the one in blue, extracted from between the blue ellipses, extending to higher energy. The CXO data appear to have resolved spatially the two spectral components (soft X-ray ionic charge exchange and hard X-ray electron bremsstrahlung) that had been previously recognized spectroscopically by XMM-Newton [*Branduardi-Raymont et al.*, 2007]. From Figures 6 and 7 it is clear that the changes in the dominant spectral component, and in the spatial morphology of the X-ray events, occur between 1 and 2 keV: this is an important clue to the acceleration mechanism acting on the aurora-generating particles.

[13] Table 1 lists results for the fitting of spectral models consisting of two, three, or four Gaussian lines plus thermal bremsstrahlung to the data in Figure 7, taking into account the effective area and energy response of the CXO telescope and the ACIS-S CCD detector. For all spectral lines, the values for σ are fixed at 20 eV, significantly less than the ACIS-S energy resolution, while the energies of the line centers and line normalizations, and the bremsstrahlung normalization, are determined by least-square fitting. The temperature of the bremsstrahlung component is not well-determined by these data because the CXO has no response above 10 keV; for these fits the bremsstrahlung temperature was fixed at 90 keV, which gives the best average approximation to the XMM-Newton spectra of Jupiter's aurorae [*Branduardi-Raymont et al.*, 2007]. The fits for three and four lines are statistically acceptable, although at somewhat different confidence levels. Also shown in Figure 7 are the best-fit models and residuals for the three line model and the four line model for the inner and outer regions, respectively. For the outer region, the improvement in the fit for the four line model over the three line model is almost entirely due to the addition of a line at ~4.1 keV, with the emitted power in this line comparable to that in the bremsstrahlung component over the energy band 2.0–8.0 keV. However, for each region application of the F-test does not significantly discriminate between the three and four line models, and the ~4.1 keV line is found to be significant at only ~1σ. The < 1 keV line energies are generally consistent with those measured by XMM-Newton and attributed to oxygen (and carbon or sulphur) ions charge exchange [*Branduardi-Raymont et al.*, 2007].

[14] Also listed for each model in Table 1 are the emitted powers in the energy bands 0.25–0.4 keV, 0.4–1.0 keV, 1.0–2.0 keV, and 2.0–8.0 keV, assuming the Jupiter–Earth

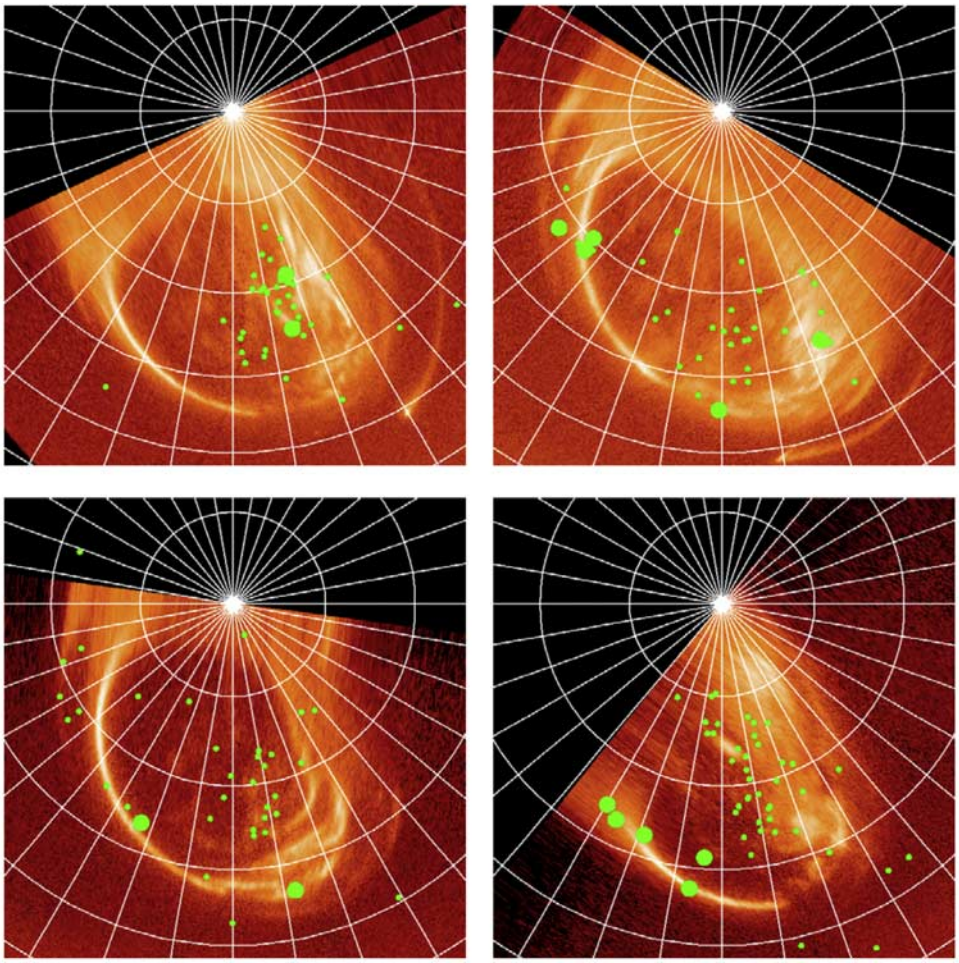

Figure 5. Polar projections as in Figure 4, but for X-ray photons collected by the CXO during individual orbits of HST; the X-ray events are overplotted on the first of several STIS exposures obtained during each HST orbit.

separation of 4.4 AU in February 2003. The quoted power values were calculated as

$$P = \int_{E_1}^{E_2} 2\pi(4.4\mathrm{AU})^2 F(E) d(E)$$

where E is the energy and $F(E)$, the energy flux at the telescope, determined from the best fit spectral model (in erg keV^{-1} cm^{-2} s^{-1}), is integrated over each energy band E_1 to E_2; the resulting values of P were then converted to MW. The power in the band 0.25–2.0 keV is ∼230 MW for the inner region but only ∼120 MW for the outer region, while the power in the band 2.0–8.0 keV is ∼9 MW for the inner region but ∼45 or 90 MW for the outer region, depending on whether the line at ∼4.1 keV is real or not.

[15] As already mentioned, a strong FUV flare was detected from the Northern aurora in February 2003 during the simultaneous CXO and Hubble STIS measurements. An associated enhancement in the 0.25–2.0 keV emission was observed, although its location on the polar cap was not the same as that of the maximum FUV intensity – attributed to electron precipitation induced by upward field-aligned currents – but was rather on its dusk side, where proton precipitation may occur (see *Elsner et al.*, 2005 for details). This shows some analogy with the events of contemporaneous variability observed by XMM-Newton at low and high X-ray energies, which indicated no clear correlation in the behavior of the ion and electron populations thought to be responsible for the emissions. A search for X-ray events at energies above 2 keV in the ACIS-S data over the period of the FUV flare has found none: if a bremsstrahlung component was present at the time, it may well have fallen below the detection threshold of CXO, given the short duration of the flare, and thus of the data integration time (∼10 min, versus the ACIS-S total observation time of ∼500 min).

3. Discussion

[16] Our re-examination of the CXO observations of Jupiter in February 2003 has led to a very important result: X-ray events with energy in excess of 2 keV in the auroral regions are found to lie spatially on the periphery of the softer X-ray events, which fall well within the polar caps. About half of the higher energy events in Jupiter's System III Northern hemisphere are co-located to a very good approximation with a section of the main FUV auroral oval around CML = 210°; the rest lie in a zone at CML = 160°

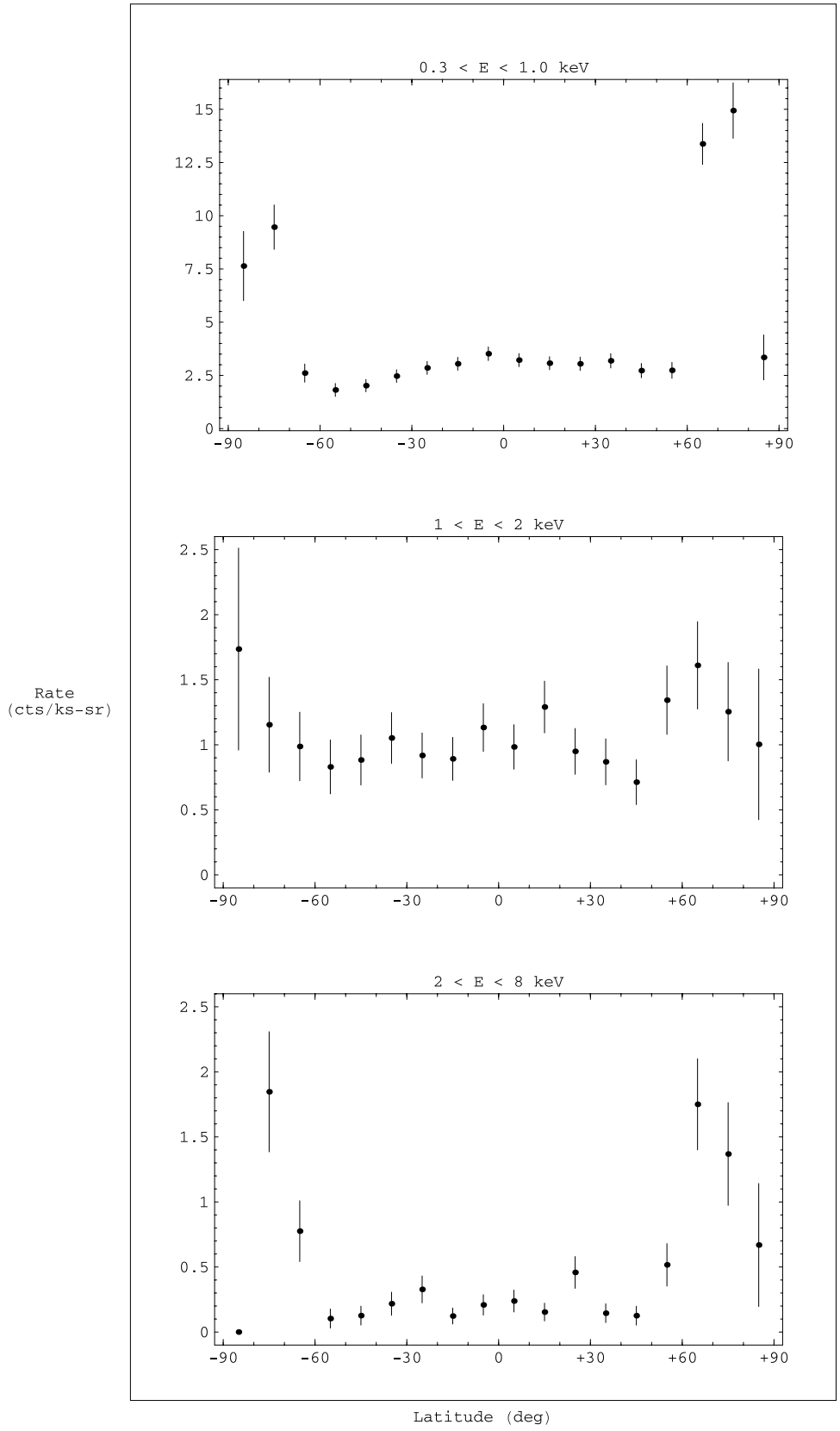

Figure 6. CXO ACIS-S count rates versus Jovian latitude in the 0.3–1.0 keV (top), 1.0–2.0 keV (middle) and 2.0–8.0 keV (bottom) energy bands. The auroral signal is very strong in both, the lowest and the highest energy bands. The small equatorial enhancement in the 0.3–1.0 keV band is a residual artifact of the "red leak' in the detector (see *Elsner et al.* [2005] for details), which occurs only at the equator and reduces with increasing energy.

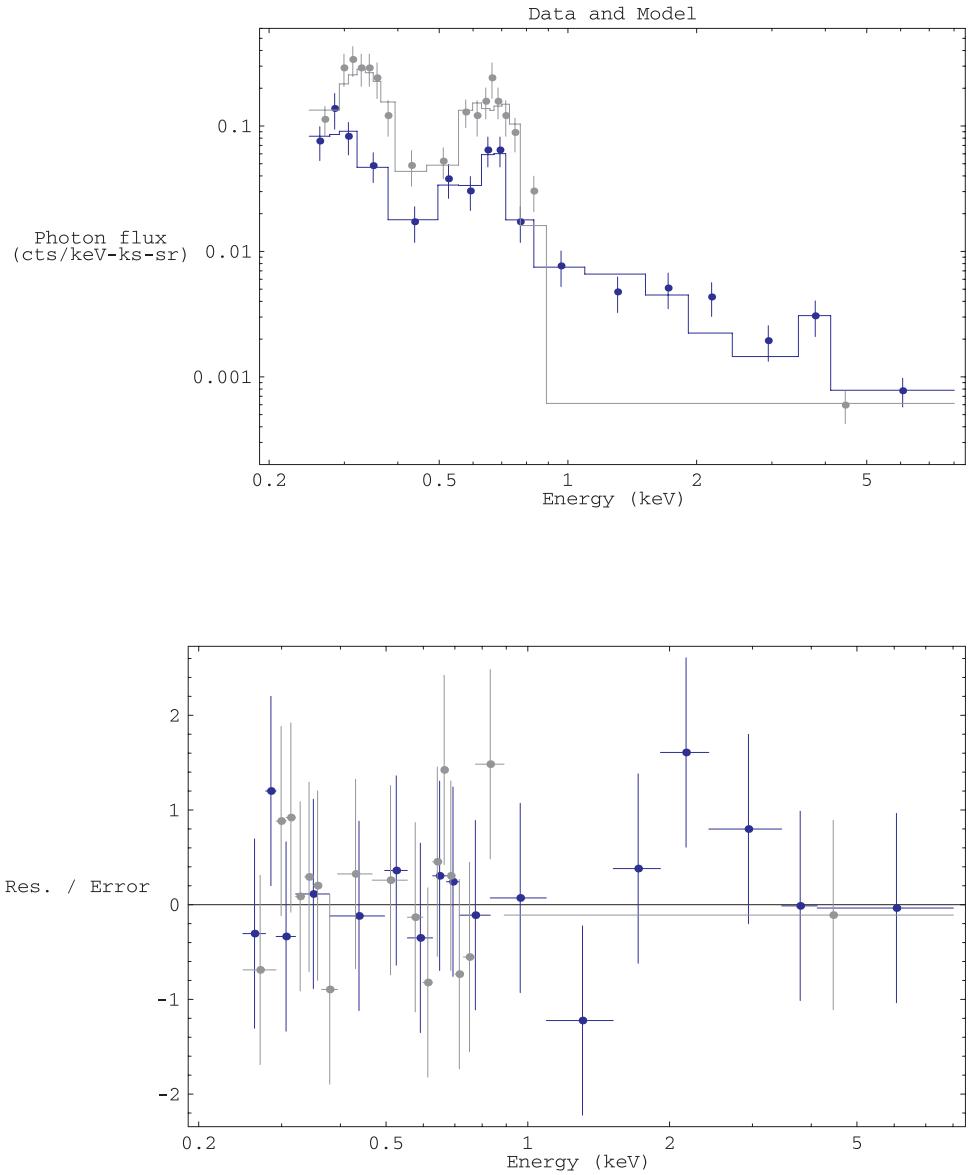

Figure 7. Top: Observed ACIS-S photon spectra (cts/keV-ks-sr) versus energy (keV) for Jupiter's Northern aurora. The spectrum for the region inside the inner blue ellipse in the top right panel of Figure 1 is shown in grey, while that for the region between the two blue ellipses is shown in blue. Note that there are no data points between 0.9 and 4 keV in the grey spectrum. Also shown are two of the spectral models listed in Table 1: (1) the 3 Gaussian line plus thermal bremsstrahlung model, with kT fixed at 90 keV, for the inner region, in grey; and (2) the 4 Gaussian line plus thermal bremsstrahlung model, with kT fixed at 90 keV, for the outer region, in blue. Bottom: Residuals (divided by the errors) for the two fits.

characterized by strong FUV emission, and extend in the general direction of the IR Bright Polar Region [*Stallard et al.*, 2003]. Bremsstrahlung emission, extending to high X-ray energies, from energetic electrons precipitating in Jupiter's aurorae had been predicted and modeled theoretically, and has been identified as such with XMM-Newton. On the other hand, FUV emission is thought to be the product of energetic electrons interacting with and exciting H and H_2 molecules, with subsequent production of H Lyα emissions and H_2 Lyman and Werner bands. Co-location of the hard X-ray and FUV emissions would be consistent with expectations as to their origins. The leading model of auroral production suggests that the breakdown of plasma co-rotation and the associated large currents generated from that process in the region around 30 R_J are the main source of electron auroral precipitation [*Cowley and Bunce*, 2001]. However, this mechanism would in general predict a uniform longitudinal distribution of aurora, whereas the concentration of X-ray events observed at System III longitude of 160° (bottom panel of Figure 3) is more consistent with the "windshield wiper' effect at Jupiter [*Herbert et al.*, 1987]: this involves high energy electrons at L = 8–12 drifting westward around Jupiter, and preferentially precipitating in regions where the magnetic field is decreasing in the drift direction and is lower than in the conjugate hemisphere. Not all the bright spots in the bottom

Table 1. Spectral Fitting Results for the Northern Aurora

Region	Inner[a]			Outer[b]		
No. of Gaussian Lines[c]	2	3	4	2	3	4
E_1, keV	0.435	0.325 ± 0.005	$0.326^{+0.005}_{-0.006}$	0.302 ± 0.009	$0.298^{+0.009}_{-0.023}$	$0.298^{+0.009}_{-0.061}$
A_1 (photon/cm^2 −s)/10^6	9.3	134^{+16}_{-14}	134^{+18}_{-15}	$68.8^{+20.4}_{-9.1}$	$61.0^{+18.3}_{-21.7}$	$61.6^{+16.1}_{-20.4}$
E_2, keV	0.681	$0.592^{+0.030}_{-0.021}$	$0.567^{+0.354}_{-0.035}$	$0.661^{+0.110}_{-0.120}$	$0.511^{+0.024}_{-0.027}$	$0.514^{+0.021}_{-0.029}$
A_2 (photon/cm^2 −s)/10^6	8.3	$8.0^{+0.9}_{-1.8}$	$5.3^{+1.6}_{-2.6}$	$5.3^{+0.7}_{-1.1}$	$2.7^{+1.2}_{-0.9}$	2.9 ± 1.0
E_3, keV	—	$0.712^{+0.039}_{-0.013}$	$0.669^{+0.026}_{-0.321}$	—	$0.671^{+0.013}_{-0.012}$	0.672 ± 0.012
A_3 (photon/cm^2 −s)/10^6	—	$5.1^{+1.6}_{-1.5}$	$6.4^{+1.7}_{-1.8}$	—	$4.3^{+1.0}_{-0.9}$	$4.4^{+1.1}_{-0.8}$
E_4, keV	—	—	$0.772^{+0.137}_{-0.028}$	—	—	$4.094^{+0.030}_{-0.032}$
A_4 (photon/cm^2 −s)/10^6	—	—	$1.6^{+1.3}_{-1.0}$	—	—	1.2 ± 0.4
A_{brems}[d,e]/10^6	1.1	1.2 ± 0.3	1.2 ± 0.7	$6.1^{+0.8}_{-0.7}$	$6.0^{+0.7}_{-0.8}$	5.3 ± 08
χ^2	92.3	9.28	4.43	21.6	14.5	6.96
ν (no. of dof)	13	11	9	12	10	9
$\chi^2_{\text{red}} = \chi^2/\nu$	7.10	0.84	0.49	1.80	1.45	0.87
Pr[$>\chi^2$] by chance	5.17e−14	0.596	0.881	0.042	0.150	0.541
P (0.25−0.4) (MW)	1.0	190	191	92.4	80.6	81.3
P (0.4−1.0) (MW)	42.8	38.0	38.7	22.3	25.5	25.3
P (1.0−2.0) (MW)	1.8	2.0	1.9	10.1	9.88	8.71
P (2.0−8.0) (MW)	7.9	9.0	8.7	45.6	44.6	90.4[f]

[a]Events confined to the region inside the inner blue ellipse in the top right panel of Figure 1.
[b]Events confined to the region between the blue ellipses and above the blue horizontal line in the top right panel of Figure 1.
[c]Values for line σ fixed at 20 eV.
[d]Values for kT fixed at 90 keV.
[e]Definition of normalization given at http://heasarc.gsfc.nasa.gov/docs/xanadu/xspec/manual/XSmodelBremss.html.
[f]The line at 4.1 keV accounts for the enhanced power in this band for this fit.

panel of Figure 3 agree with this scheme, but the ones in the Northern hemisphere near the labels '9', '11', and '13' (which indicate surface magnetic field strength in Gauss on the nearest contour) and the ones in the Southern near the label '11' seem to agree with this scenario quite well, supporting the view that the particles involved are most likely electrons.

[17] To test quantitatively the possibility that the electrons radiating bremsstrahlung X-rays over the auroral regions are also responsible for the FUV emission we have used the models of *Singhal et al.* [1992] to predict the powers generated by the electrons in the two bands, and we have compared them with those derived from the CXO/HST observations. Application of the Singhal et al. calculations seems appropriate because they have shown to be a good match of the auroral high energy X-ray spectrum measured during XMM-Newton observations [*Branduardi-Raymont et al.*, 2007]. Adopting an electron energy of 100 keV (close to the value of 90 keV assumed for the fits to the ACIS-S data) and integrating the corresponding particle distribution in Figure 5 of Singhal et al., we obtain an expected 2.0−8.0 keV power of 11 MW. From their Table 3 we also infer that the FUV power emitted by the same electrons, before absorption in the atmosphere, is of the order of 1500 GW, for an auroral area of 10^{19} cm^2. This implies that the power in the FUV emission is predicted to be some 10^5 times that in the hard X-rays. However, the modeling results of *Waite et al.* [1992] imply an efficiency factor for X-ray production about a factor of 5−10 lower than that of *Singhal et al.* [1992], so the FUV power could be up to 6 orders of magnitude larger than that in the X-rays.

[18] From the February 2003 ACIS-S and STIS observations of the Northern aurora we have derived a 2.0−8.0 keV power of 45 MW due to bremsstrahlung for the strip where most of the > 2 keV emission is located, and an average emitted FUV power of 340 GW, which is $\sim 10^4$ times the hard X-ray power. This is clearly a very approximate estimate of two quantities of very different magnitude; nevertheless, the fact that the relative powers of the hard X-ray and FUV emissions from Jupiter's Northern aurora are within a factor of 10 of model predictions [*Singhal et al.*, 1992] can be taken as giving support to the idea that the same electrons produce the emissions in the two bands.

[19] There is an additional very important point to consider. The fact that the electron bremsstrahlung efficiency is so low suggests that if we see hard X-rays, they must relate to bright aurorae: these are associated with either brightenings in the dawn auroral oval [*Gérard et al.*, 2003], phenomena like the midnight tail reconnection burst seen by *Grodent et al.* [2004], just poleward of the nightside auroral oval, or the flare effect [*Waite et al.*, 2001], which occurs inside the auroral oval proper. At least in case of the flares, the brightenings are likely to be associated with solar wind interaction effects [*Waite et al.*, 2001; *Pallier and Prangé*, 2004]. Furthermore, *Elsner et al.* [2005] observed the soft X-rays brighten along the dusk flank when the FUV flare occurred. Therefore it may be no surprise that the bremsstrahlung electrons are correlated, at least on occasions, with the low energy X-rays and in turn with solar wind interaction.

4. Conclusions

[20] Observations of Jupiter's aurorae with the CXO show that the spatial distribution of the X-ray events is dependent on their energy, and thus on the energetic particles thought to be responsible for their emission: we find that the 2.0−8.0 keV events, identified as electron bremsstrahlung, lie at the periphery of those in the range 0.3−2.0 keV, originating from ionic charge exchange, and

are co-located with bright FUV auroral regions. This morphological evidence, the spectral shape of the high energy X-ray component, and the broad consistency of the relative hard X-ray and FUV powers of the Northern aurora with model predictions, all support the idea that the same energetic electrons are responsible for both the hard X-ray and the FUV emissions from Jupiter's auroral regions.

[21] **Acknowledgments.** G. Branduardi-Raymont acknowledges financial support from the UK Science and Technology Facilities Council (STFC). D. Grodent is supported by the Belgian Fund for Scientific Research (FNRS) and by the PRODEX Program managed by the European Space Agency in collaboration with the Belgian Federal Science Policy Office. This work was supported in part by guest observer grants from the Chandra X-ray Center. We also warmly thank R. Prangé for useful discussions.

[22] Wolfgang Baumjohann thanks Konrad Dennerl and another reviewer for their assistance in evaluating this paper.

References

Bhardwaj, A., and G. R. Gladstone (2000), Auroral emissions of the giant planets, *Rev. Geophys.*, *38*, 295–353.

Bhardwaj, A., R. F. Elsner, G. R. Gladstone, J. H. Waite Jr., G. Branduardi-Raymont, T. E. Cravens, and P. Ford (2006), Low- to middle-latitude X-ray emission from Jupiter, *J. Geophys. Res.*, *111*, A11225, doi:10.1029/2006JA011792.

Bhardwaj, A., et al. (2007), X-rays from solar system bodies, *Planet. Space Sci.*, *55*(9), 1135–1189, doi:10.1016/j.pss.2006.11.009.

Branduardi-Raymont, G., R. F. Elsner, G. R. Gladstone, G. Ramsay, P. Rodriguez, R. Soria, and J. H. Waite Jr. (2004), First observation of Jupiter by XMM-Newton, *Astron. Astrophys.*, *424*, 331–337, doi:10.1051/0004-6361:20041149.

Branduardi-Raymont, G., A. Bhardwaj, R. F. Elsner, G. R. Gladstone, G. Ramsay, P. Rodriguez, R. Soria, J. H. Waite Jr., and T. E. Cravens (2007), A study of Jupiter's aurorae with XMM-Newton, *Astron. Astrophys.*, *463*, 761–774, doi:10.1051/0004-6361:20066406.

Broadfoot, A. L., et al. (1979), Extreme ultraviolet observations from Voyager 1 encounter with Jupiter, *Science*, *204*, 979–982.

Connerney, J. E. P., M. H. Acuna, N. F. Ness, and T. Satoh (1998), New models of Jupiter's magnetic field constrained by the Io flux tube footprint, *J. Geophys. Res.*, *103*, A11929, doi:10.1029/97JA03726.

Cowley, S. W. H., and E. J. Bunce (2001), Origin of the main auroral oval in Jupiter's coupled magnetosphere-ionosphere system, *Planet. Space Sci.*, *49*, 1067–1088.

Elsner, R. F., et al. (2005), Simultaneous Chandra X-ray, Hubble Space Telescope ultraviolet, and Ulysses radio observations of Jupiter's aurora, *J. Geophys. Res.*, *110*, A10207, doi:10.1029/2004JA010717.

Gérard, J.-C., J. Gustin, D. Grodent, J. T. Clarke, and A. Grard (2003), Spectral observations of transient features in the FUV Jovian polar aurora, *J. Geophys. Res.*, *108*(A8), 1319, doi:10.1029/2003JA009901.

Gladstone, G. R., et al. (2002), A pulsating auroral X-ray hot spot on Jupiter, *Nature*, *415*, 1000–1003.

Grodent, D., J. H. Waite Jr., and J.-C. Gérard (2001), A self-consistent model of the Jovian auroral thermal structure, *J. Geophys. Res.*, *106*, 12,933–12,952, doi:10.1029/2000JA900129.

Grodent, D., J.-C. Gérard, J. T. Clarke, G. R. Gladstone, and J. H. Waite Jr. (2004), A possible auroral signature of a magnetotail reconnection process on Jupiter, *J. Geophys. Res.*, *109*, A05201, doi:10.1029/2003JA010341.

Gustin, J., J.-C. Gérard, D. Grodent, S. W. H. Cowley, J. T. Clarke, and A. Grard (2004), Energy-flux relationship in the FUV Jovian aurora deduced from HST-STIS spectral observations, *J. Geophys. Res.*, *109*, A10205, doi:10.1029/2003JA010365.

Herbert, F., B. R. Sandel, and A. L. Broadfoot (1987), Observations of the Jovian Aurora by Voyager, *J. Geophys. Res.*, *92*, 3141–3154.

Hurley, K., M. Sommer, and J. H. Waite Jr. (1993), Upper limits to Jovian hard X radiation from the ULYSSES gamma ray burst experiment, *J. Geophys. Res.*, *98*, 21,217–21,219.

Pallier, L., and R. Prangé (2004), Detection of the southern counterpart of the Jovian northern polar cusp: Shared properties, *Geophys. Res. Lett.*, *31*(6), L06701, doi:10.1029/2003GL018041.

Sandel, B. R., D. E. Shemansky, A. L. Broadfoot, J. L. Bertaux, J. E. Blamont, M. J. S. Belton, J. M. Ajello, J. B. Holberg, S. K. Atreya, and T. M. Donahue (1979), Extreme ultraviolet observations from Voyager 2 encounter with Jupiter, *Science*, *206*, 962–966.

Singhal, R. P., S. C. Chakravarty, A. Bhardwaj, and B. Prasad (1992), Energetic electron precipitation in Jupiter's upper atmosphere, *J. Geophys. Res.*, *97*, 18,245–18,256.

Stallard, T. S., S. Miller, S. W. H. Cowley, and E. J. Bunce (2003), Jupiter's polar ionospheric flows: Measured intensity and velocity variations poleward of the main auroral oval, *Geophys. Res. Lett.*, *30*(5), 1221, doi:10.1029/2002GL016031.

Waite, J. H., Jr., D. C. Boice, K. C. Hurley, S. A. Stern, and M. Sommer (1992), Jovian bremsstrahlung X-rays: A Ulysses prediction, *Geophys. Res. Lett.*, *19*, 83–86.

Waite, J. H., et al. (2001), An auroral flare at Jupiter, *Nature*, *410*, 787–789.

G. Branduardi-Raymont, Mullard Space Science Laboratory, University College London, Holmbury St Mary, Dorking, Surrey, RH5 6NT, UK. (gbr@mssl.ucl.ac.uk)

T. E. Cravens, Department of Physics and Astronomy, University of Kansas, Lawrence, KS 66045, USA.

R. F. Elsner, NASA Marshall Space Flight Center, NSSTC/XD12, Space Science Branch, 320 Sparkman Drive, Huntsville, AL 35805, USA.

P. Ford, Massachusetts Institute of Technology, Kavli Institute for Astrophysics and Space Research, 70 Vassar Street, Cambridge, MA 02139, USA.

M. Galand, Imperial College London, Space and Atmospheric Physics Group, Blackett Laboratory, Prince Consort Road, London, SW7 2BW, UK.

G. R. Gladstone and J. H. Waite Jr., Southwest Research Institute, 6220 Culebra Road, San Antonio, TX 78228-0510, USA.

D. Grodent, Laboratoire de Physique Atmosphérique et Planétaire, Institut d'Astrophysique et de Géophysique, Université de Liège, Avenue de Cointe 5, B-4000 Liège, Belgium.